Automotive and Engine Technology (2025) 10:7
https://doi.org/10.1007/s41104-025-00152-y

ORIGINAL PAPER

Influence of surfaces of different chemical composition and topology on the interaction between a fuel-spray and an oil-wetted wall

Celine Krnac[1] · Jan Reimer[1] · Malki Maliha[1] · Heiko Kubach[1] · Thomas Koch[1]

Received: 3 April 2025 / Accepted: 9 May 2025

Abstract
The combustion anomaly of pre-ignition presents a particular challenge, especially in downsized engines. The interaction between the injected fuel and the oil-wetted cylinder wall plays a central role in the formation of reactive deposits, which are suspected of promoting pre-ignition. This paper investigates the influence of different tribological cylinder surfaces on this interaction. Plates with different surface properties are used and analysed using laser-induced fluorescence and optical measurements. The results will help to understand how surface properties influence the fuel-oil interaction and thus the probability of pre-ignition.

Keywords Pre-ignition · Fuel-wall-interaction · Chemical composition · Topology · LIF · Secondary droplets

Abbreviations

2D	Two-dimensional
3D	Three-dimensional
CCD	Charge-coupled device
CMOS	Complementary Metal-Oxide-Semiconductor
CO_2	Carbon dioxide
i.e	Id est (that is)
LED	Light-emitting diode
LIF	Laser-induced fluorescence
l_m	Measuring section
MPD	Multi-pinhole disc
PTV	Particle tracking velocimetry
R_a	Arithmetic mean roughness value
RGB	Red, green, blue
RON	Research octane number
R_z	Average roughness depth
S_0	Ground energie level
S_1	Excited energy level
S_a	Arithmetical mean height
TTL	Transistor-transistor logic
W	Watt

✉ Celine Krnac
uifkj@student.kit.edu

Jan Reimer
jan.reimer@kit.edu

Malki Maliha
malki.maliha@kit.edu

Heiko Kubach
heiko.kubach@kit.edu

Thomas Koch
thomas.a.koch@kit.edu

[1] Karlsruhe Institute of Technology, Karlsruhe, Germany

1 Introduction

Due to climate change, the emission standards for internal combustion engines are becoming more stringent, especially in the reduction of CO_2 emissions. To archieve a reduction in CO_2 emissions, downsizing of internal combustion engines has been established and is gaining in importance. To achieve the same power with a smaller engine displacement, the specific power must increase. In addition to the intentional combustion of the air-fuel mixture, which is ignited by an ignition spark, abnormal combustion can also occur. Combustion anomalies are more commonly observed in highly charged gasoline engines with direct injection. A better understanding of these anomalies is therefore particularly important. They are divided into knocking, glow ignition and pre-ignition. In the case of pre-ignition, uncontrolled self-ignition of the unburned air-fuel mixture occurs before ignition by the spark plug [1]. This creates high pressures and temperatures in the combustion chamber. This can lead to knocking, which can damage the engine. The unwanted interaction between the injected fuel and the oil-wetted cylinder wall is suspected to be the trigger for pre-ignition in

Published online: 30 May 2025

addition to the influence on pollutant emissions. In the literature, internal engine deposits are mentioned as a possible ignition source during pre-ignition [1]. Compared to fuel-based deposits, which are predominantly organic, oil-based deposits consist of non-organic substances such as calcium or zinc. According to Schweizer, these oil-based deposits have a higher reactivity and therefore a higher probability of triggering pre-ignition [2]. They are primarily formed by the interaction between the injected fuel and the oil-wetted cylinder wall in the combustion chamber. If the fuel jet interacts more strongly with the oil film, this has been shown to increase the probability of pre-ignition [3].

It is therefore important to have a good understanding of the variables that reduce or increase the probability of pre-ignition. With the increasing use of downsized engines, this interaction is becoming more and more important. This paper presents the influence of different tribological cylinder surfaces on this interaction. Three plates with different surface characteristics are used to simulate different cylinder surfaces. Oil and fuel are mixed with tracers so that the interaction can be visualised using laser-induced fluorescence. The interaction is analysed optically using images from high-speed and low-speed cameras.

2 State of knowledge

2.1 Droplet-fluid-interaction

In combustion engines with direct injection, the injected fuel can interact with the oil-wetted cylinder wall during the injection process. The injected fuel evaporises in the combustion chamber after injection. However, if the fuel does not have enough time to evaporate or the temperature is below the boiling point, droplets of fuel that are still liquid will reach the oil film on the cylinder wall and interact with it.

These interactions result in the formation of various phenomena, will be discussed in more detail below. Maliha [4] divides these phenomena into fog, wave, fuel enrichment and secondary droplets, which are shown in Fig. 1 and characterised below.

Immediately after the fuel jet hits the oil film, a fog is formed, which consists of a large number of droplets. Maliha's optical tests could not determine the exact composition of the fog. The movement of these very small droplets takes place in the positive x-direction, parallel to the oil film surface (see Fig. 1) and has a propagation speed of about 15 m/s at an injection pressure of 50 bar. The reason for this is that the injected fuel jet stimulates the undisturbed atmospheric air and causes a flow in the positive x-direction. The impinging fuel jet creates waves in the oil film, which propagate in the positive x-direction during and shortly after the end of injection.

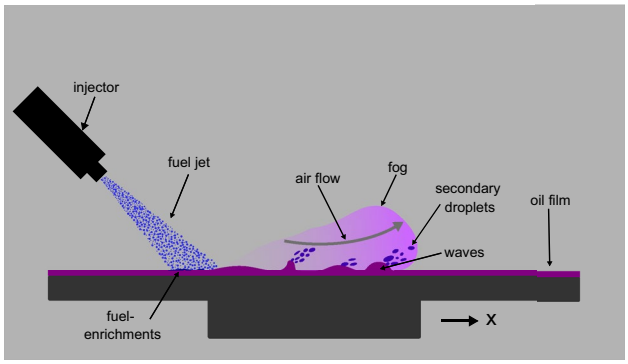

Fig. 1 Droplet-fluid-interaction and the phenomena involved

Fuel enrichment occurs in areas where the spray meets the oil film, as shown in Fig. 3. The transfer of kinetic energy from the fuel jet to the oil film slows down the fuel droplets and leads to fuel enrichment. Accordingly, fuel enrichment can be observed on the surface of the oil film at the end of injection. The air flow induced by the fuel jet causes the oil film to be locally affected by a flow or shear force, which can cause large droplets to detach from the wave peaks. The air flow induced by the fuel jet causes the oil film to be locally influenced by a flow or shear force, which is why large droplets can detach from the wave peaks. These move parallel to the surface of the oil film and are called secondary droplets. The secondary droplets are many times larger than the fog droplets, as shown in Fig. 1, and have a size between 40 µm and 360 µm. However, they only move in the positive x-direction at a speed of about 10 m/s. These droplets are mainly composed of fuel [4].

2.2 Adhesion and surface energy

The adhesive forces between the oil and the cylinder liner are stronger than the cohesive force that causes the oil to stick to the surface. Adhesive forces are attractive forces between different molecules, whereas cohesive forces are attractive forces between molecules of the same type [5]. There are various theories and subdivisions in the literature to describe the causes of adhesion. They are often divided into mechanical and specific adhesion [6]. Mechanical adhesion occurs on rough surfaces. A form-fitting connection in the surface structures, such as cracks and pores, of the wetted surface with the liquid [7]. According to Flock, a rougher surface can lead to an increase in the importance of mechanical adhesion by increasing the active surface area [7]. Specific adhesion is subdivided into physical, chemical and thermodynamic phenomena [7–9]. These theories emphasise various interactions, such as van der Waals

forces, covalent bonds and the formation of dipoles and electrical double layers.

The tendency of materials to form interfaces and interact with others is influenced by surface energy. It describes the amount of energy required per unit area to form a surface. A liquid medium tends towards the most energetically favourable state, resulting in complete wetting of the surface, as less energy is required at the phase boundary than in the interior of the medium. A liquid medium tends towards the most energetically favourable state, which leads to complete wetting of the surface, because less energy is required at the phase boundary than inside the medium. How well a liquid forms an interface with a solid is known as wettability. The surface energy of a substance has a major influence on its wettability. Accordingly, substances have better wettability if the surface energy of the wetted material is higher [7].

2.3 Tribology

Tribology, the study of friction, wear and lubrication [10], is of great importance in internal combustion engines. It is closely related to the factors that influence the interaction between fuel, oil and cylinder surfaces. Piston rings are used in the engine to seal the combustion chamber from the crankshaft housing and reduce the amount of oil on the cylinder wall. In the process, the piston rings come into contact with the cylinder surface. The relative movement of the piston causes high friction between the piston rings and the cylinder surface. This makes the presence of a lubricating film essential. The separation of the piston rings and the cylinder bore by a thin film of oil reduces friction losses and wear and ensures better sliding properties. The cylinder liner is the base body and the piston rings are the mating body. The way in which the base and mating bodies come into contact can be categorised into different types of friction. The complete separation of the two solid bodies by a liquid intermediate medium is referred to as fluid friction [10]. If the liquid film is completely removed, the two solids come into direct contact, which is known as dry friction [10]. When the lubricant film between two solid surfaces is too thin to separate them completely, this is called boundary friction. Boundary friction occurs where speeds are so low or lubricant supply is insufficient that the hydrodynamic effect of the lubricant is negligible [10]. Mixed friction is a combination of the two types of friction described above, i.e. boundary friction and fluid friction [10]. Fluid friction occurs between the piston rings and the cylinder mating surface in the areas between the top and bottom dead centre [11]. This is where the piston has a high relative speed, causing it to slide on the lubricating film. As its speed decreases in the top and bottom dead centre areas, the thickness of the oil film is reduced [11]. Mixed friction occurs in these areas.

The surface finish of the base body—the cylinder bore—has a major influence on the behaviour of the lubricant film. A basic distinction must be made between the geometric, real and effective surfaces. The geometric surface is the ideal surface, which can be taken from the dimensions of the technical drawings. In reality, in addition to the geometric surface, there is also the surface created by surface roughness. This is known as the real surface. If the real solid surface is wetted with a lubricating film, the effective surface is created [12].

3 Roughness examination with a confocal microscope

3.1 Roughness values

A confocal microscope can be used to optically measure surface properties such as roughness or layer thickness. This non-contact, optical measurement method allows the surface of various materials to be recorded in two or three dimensions in the micro- and nanometre range. The ‘µsurf expert’ confocal microscope from NanoFocus was used to measure the surface roughness.

A multi-pinhole disc (MPD) and lens are used to focus the light rays from the built-in LED onto the surface to be inspected. After hitting the surface, the light is reflected and passes through the pinhole of the MPD onto the CCD sensor. This ensures that only the reflected light from the focused area hits the CCD sensor. The intensity of the reflected light is measured for each illuminated area. By moving the surface towards the lens, images can be taken in sections for each focal point, allowing the entire surface to be scanned. The resulting images are combined to create a three-dimensional surface profile, as shown in Fig. 2 for a rough aluminium surface. Using the same company's µsoft analysis software, it is possible to extract the required parameters or roughness profiles from the images of the surface to enable the images to be analysed.

To make statements about the roughness of the surface, different roughness values can be determined. To make statements about the roughness of the surface, different roughness values can be determined. These include the average roughness depth R_z and the arithmetic mean roughness R_a of a two-dimensional section of the surface or the arithmetic mean height S_a of the entire measured surface. These are given in Table 1.

3.2 Confocal Microscope Results

To investigate the interaction between the injected fuel and the cylinder wall, three different sample plates were prepared. Their surface properties were analysed using the

confocal microscope described above. The first plate was made of aluminium. The second plate is made of the same material but with a roughened surface to investigate the influence of surface roughness on the interaction. The third plate is made of grey cast iron and is compared with the smooth aluminium plate to study the influence of different chemical compositions on the behaviour during the interaction in more detail. In all images taken with the confocal microscope, a selected area of the surface, approximately 15.2 x 15.1 mm, was observed, see Fig. 3.

The resolution is 11176 x 11185 pixels, so one pixel has a size of 1.36 µm in the x-direction and 1.35 µm in the y-direction. The 1600S objective was used for the images with the confocal microscope and an exposure time of 40 ms was selected. A step size in the z-direction of 0.937 µm was used for the three plates. Table 2 shows the previously described roughness values S_a, R_a and R_z for the different plates. It can

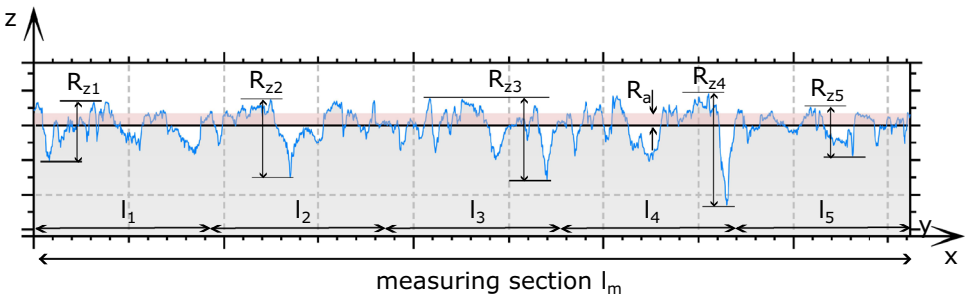

Fig. 2 Roughness values

Tabel 1 Roughness values acording to [6, 13]

Roughness values	Description
Average roughness depth R_z	Determined by dividing the roughness profile into 5 equal sections and determining the maximum profile depth of each section. The mean value gives R_z
Arithmetic mean roughness value R_a	Integral of the deviations of the roughness profile from the centre line. Shown as a rectangular surface
Arithmetic mean height S_a	The mean value of the height deviations over the entire measured surface

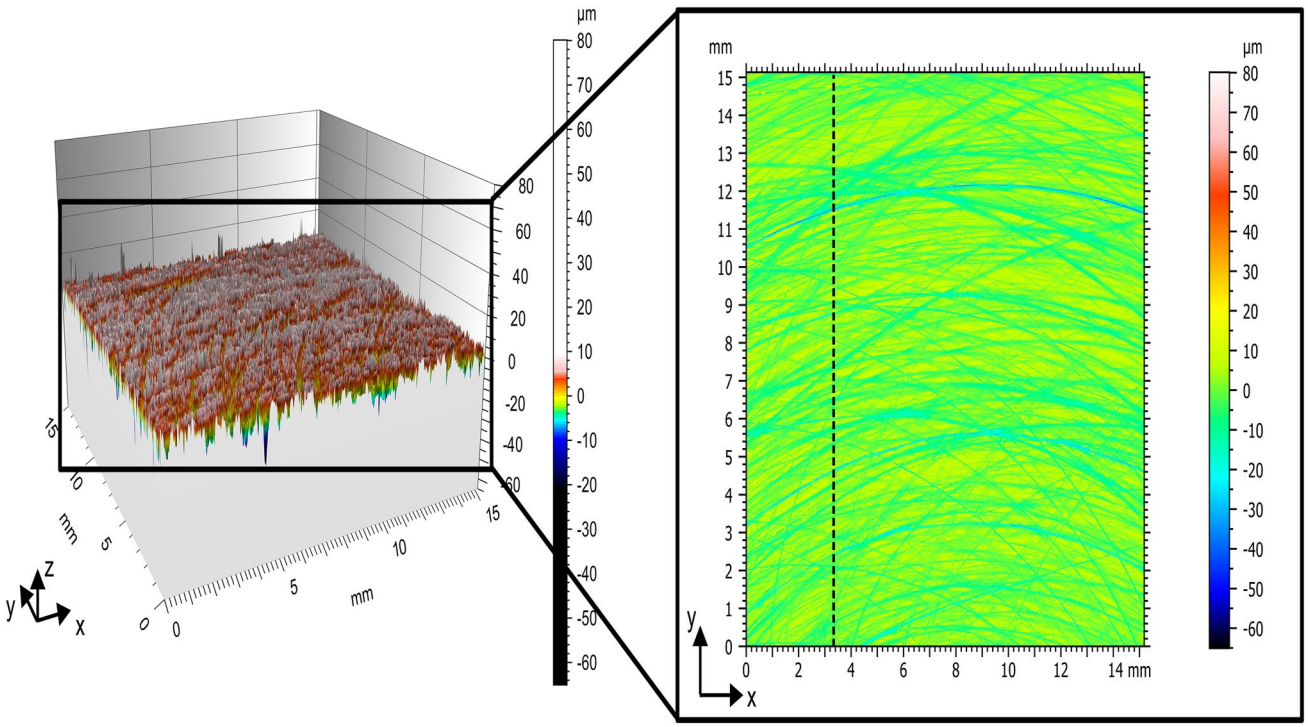

Fig. 3 3D and 2D surface of the rough aluminium plate

Tabel 2 Arithmetic mean height S_a, arithmetic mean roughness R_a, average roughness depth R_z of the smooth and rough aluminium plate and the grey cast iron plate

	Arithmetical mean height S_a [µm]	Arithmetic mean roughness value R_a [µm]	Average roughness depth R_z [µm]
Smooth aluminium plate	0.499	0.435	3.82
Rough aluminium plate	3.15	2.14	21.4
Grey cast iron	1.26	0.997	9.91

be seen here that the values of the mean arithmetic height S_a assume different values for the surfaces of the entire selected area. As expected, the smooth aluminium surface has the smallest S_a value of 0.488 µm in the examined plate area. The rough aluminium surface has a S_a value of 3.15 µm and grey cast iron is in between at 0.997 µm. From this, it can be concluded that the roughened aluminium surface has the greatest roughness.

A roughness profile was now selected for each plate in the analysed area. This is shown as an example in Fig. 3 for the rough aluminium surface and is represented by the dashed line. The three-dimensional surface of the selected examination area of the plate can be seen on the left in Fig. 3. From this, an arbitrary section was created using the µsoft analysis software, which allows a two-dimensional roughness profile to be generated along this section, see Fig. 5.

The values of R_a and R_z were determined for these profiles and are summarised in Table 2. As shown in Table 2, the R_a value, like the S_a value, is lowest for the smooth aluminium surface at 0.435 µm. The R_a value of the grey cast iron plate in the selected plane is 0.997 µm and the R_a value of the roughened aluminium is 2.14 µm. The deviations between the S_a and R_a values of each material surface can be explained by the fact that the surface structure is not the same at every point. The deviations between the S_a and R_a values of the respective material surface can be explained by the fact that the surface structure is not the same at every point. This results in different values depending on whether the whole surface or just one plane is considered. Similarly, when looking at the R_a value of a plane, larger indentations may not be in the selected plane and will not be included in the value. The last value considered is the average roughness depth R_z. The roughness depth is lowest for the smooth aluminium surface at 3.82 µm. The roughened aluminium has the greatest roughness depth at 21.4 µm and the grey cast iron is between the two aluminium surfaces at 9.91 µm (see Table 2). The R_z value shows that the roughened aluminium plate has the greatest distance from the highest point of the surface to the lowest point. This confirms the assumption that the roughened aluminium plate has the greatest roughness. This is also evident from the roughness profiles in Fig. 4 where the values of the peaks and valleys of the profile of the roughened aluminium plate are the highest.

4 Experimental setup

To investigate the fuel-oil film interaction, an optical test setup is set up. Fig. 5a shows the actual test setup, while Fig. 5b shows the corresponding schematic diagram. To simulate the lubricating film, Total Quartz 700 EGY10 W40(SN) engine oil is poured onto a circular plate (5). An electric motor (7) is used to rotate the plate. The resulting centrifugal force removes the excess oil and produces a constant oil film thickness. The oil film thickness can therefore be adjusted to an accuracy of a few µm via the speed of the plate [4]. The Bosch HDEV 5.2 injector (3) is a direct injection injector with an electromagnetic valve and a multi-hole nozzle. To obtain a single fuel jet, five of the six injector nozzles are sealed with a fuel-insoluble two-component epoxy-based adhesive. The required fuel injection pressure is provided by a pressure accumulator (2). The fuel used is RON 95 petrol. To obtain the best possible fluorescence, the oil-wetted plate is illuminated from above by a light source (4). The light source consists of four LEDs (IN-C68QA(X) TM UV) manufactured by Inolux with a maximum electrical power of 10 W. These have been electrically connected in series to increase the light intensity. An aspherical lens (ACL2015U-A) is placed in front of the LEDs to reduce the beam angle and increase the intensity of the light beam. An optical diffuser is placed after the aspherical lens to provide uniform illumination of the interaction area. The optical diffuser is followed by a cylindrical lens that focuses the light beam and creates an intensity curve similar to a light section. The interaction is analysed from the side using the Vision Research Phantom v1612 high-speed camera with CMOS sensor (1). With this camera, it is possible to take pictures with a resolution of 1200 x 800 pixels. The E-Lite 5M low-speed camera from LaVision with a CCD sensor is used to observe the interaction area immediately after the end of the injection (6). It has a resolution of 2448 x 2050 pixels. The phantom camera is connected to a TTL trigger (9) for the side shots. This trigger first starts the shots and then triggers the injection. Both the cameras and the trigger are connected to a computer (8). The procedure for taking pictures with the E-lite is analogue.

Laser-induced fluorescence (LIF) is used to optically analyse the interaction with the experimental setup as described. Light can be absorbed, transmitted or reflected. Absorption

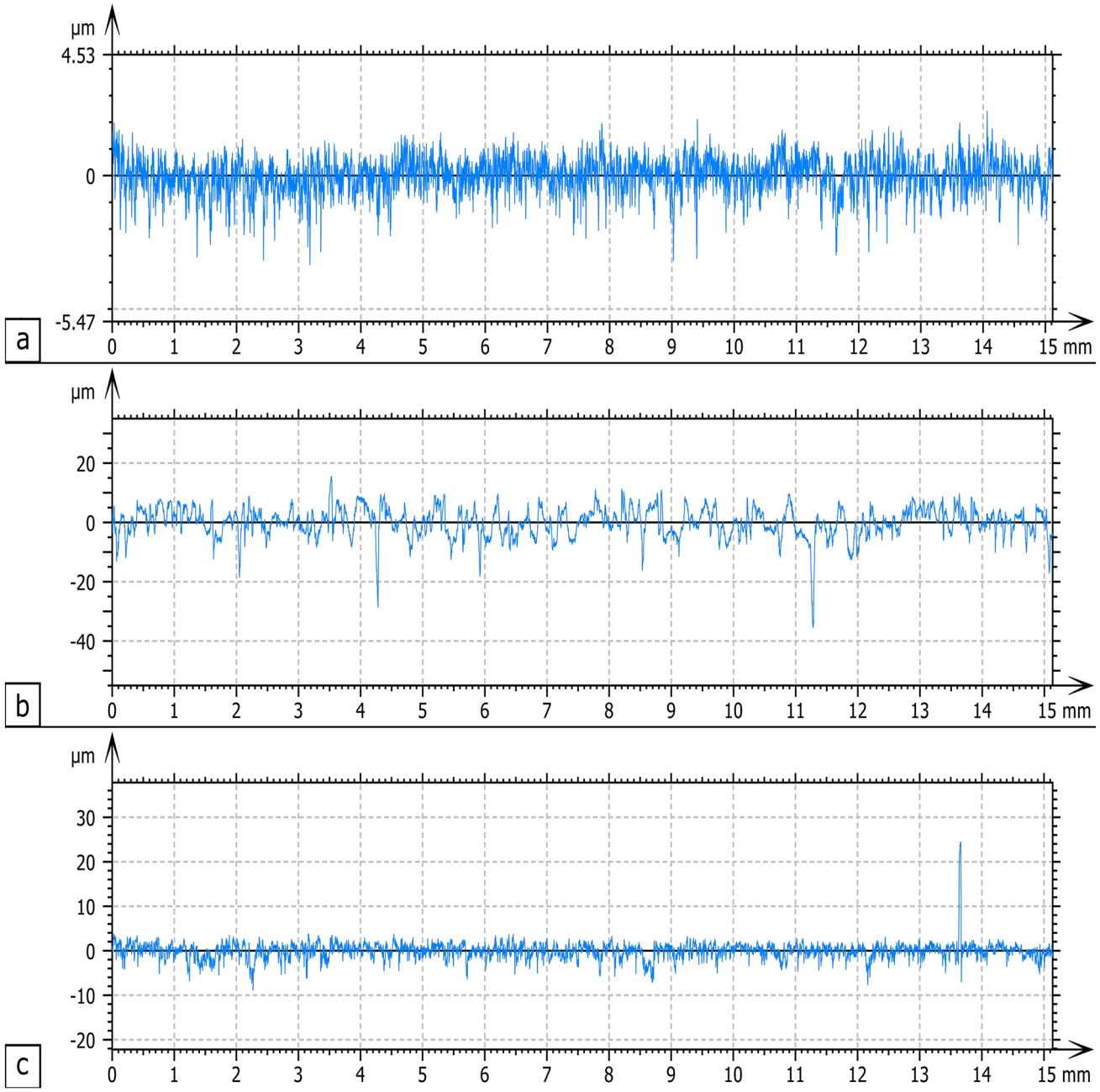

Fig. 4 Roughness profiles of the **a** smooth aluminium plate, **b** rough aluminium plate and **c** grey cast iron plate

is particularly important in LIF. In absorption, a photon transfers its energy, h*ν, to an electron. This raises the electron from its ground state S_0 to a higher energy level S_1 (Fig. 6). Vibrational relaxation allows the electron to fall from the excited state S_1 to a lower vibrational level. From there, it falls back to the more stable ground state S_0. This can happen either by quenching, i.e. transferring energy to a neighbouring electron, or by spontaneous emission of a photon. Due to voltage relaxation, the electron is at a lower energy level than immediately after absorption. Accordingly, the fluorescence emission has less energy than the energy of the absorbed photon. As a result, the wavelength of the emission is shifted relative to the wavelength of the absorption, the so-called Stokes shift (Fig. 6). The Stokes shift allows the excitation and fluorescence spectra to be spectrally separated.

A tracer is added to each of the two media, oil and fuel, to make them visible. These increase the stokes shift and the fluorescence intensity. It is very important that the spectra of the two media are very different after the addition of

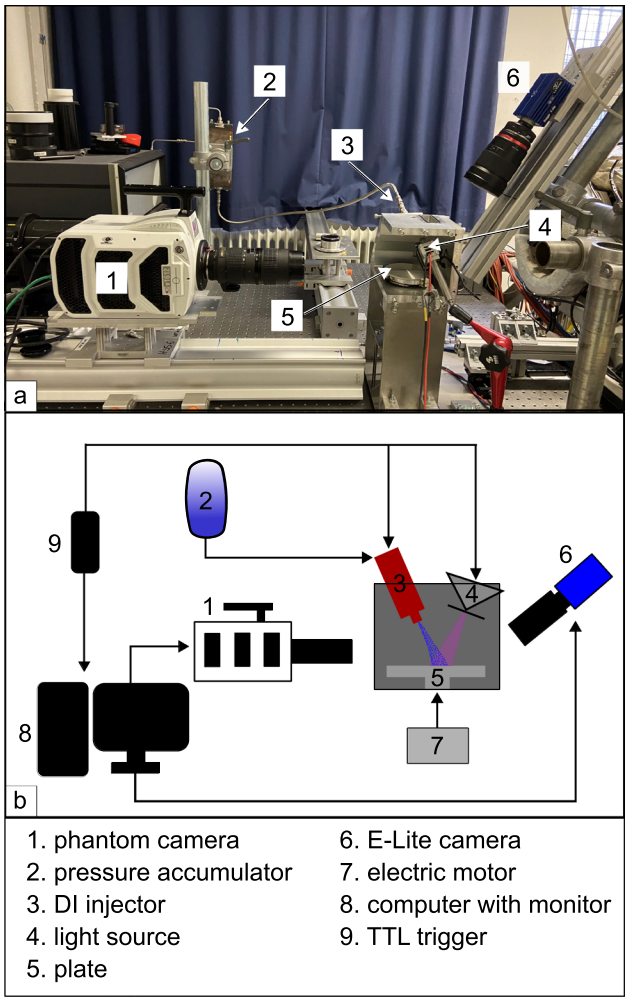

Fig. 5. Measurement setup **a** real, **b** schematic diagram

the tracers. This allows a good optical separation of fuel and oil during the interaction. [4] The Lumilux Blue tracer has a fluorescence maximum in the wavelength range below 550 nm, while the pyrromethene tracer has a fluorescence maximum below 650 nm. Furthermore, Lumilux Blue in fuel and pyrromethene dissolved in oil have mutually compatible absolute fluorescence intensities.

Four different series of measurements were selected for the tests. These parameter variations are shown in Table 3. Within the series, the oil temperature is varied between two values, 293 K and 363 K, with two different oil film thicknesses of 20 µm and 80 µm. In all four combinations, the oil film was applied to different plate surfaces already analysed in Chapter 2: smooth aluminium, rough aluminium and grey cast iron.

5 Results of impact on a oilfilm on different topological and chemical composition surfaces

5.1 Investigation of droplet detachment during fuel injection

The influence of surface roughness and chemical composition on the interaction is analysed below. The plate surfaces mentioned in Chapter 2 have been analysed for roughness and serve as the basis for this analysis. However, this analysis does not include all parameter variations for which images were taken, but only those that show a significant visible difference. Fig. 7 shows the interaction of measurement series 2 and 4 (Table 3), using the smooth aluminium plate as a representative surface.

To investigate the interactions, the droplet velocities were first determined. The images were taken at a frame rate of 10 kHz with an exposure time of 100 µs per frame. It is assumed that the secondary droplets are spherical as shown in 1.1. Similar to Particle Tracking Velocimetry (PTV), a method is used in which the liquids are marked with tracers

Fig. 6 Stokes-shift

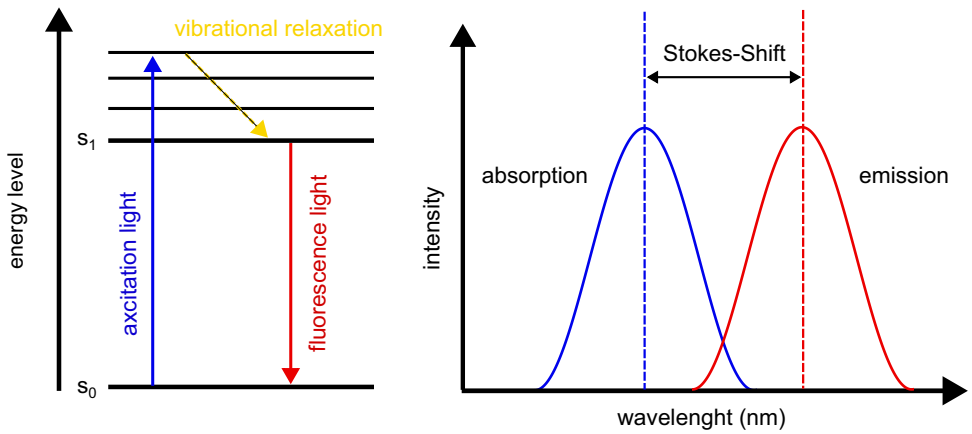

to visualise the movement of individual particles. During the exposure time, the droplets move at a certain speed, causing them to appear as short streaks on the images. The velocity of the droplets can be calculated from the length of these stripes and the known exposure time. It was found that there were no significant differences between the different plate surfaces in terms of droplet velocity. However, the oil droplets slow down towards the end of the injection. This is due to the decreasing air flow and the weaker impulse of the fuel jet. For example, the velocity in measurement series 4, see Table 3, decreases from about 15–20 m/s to about 8–12 m/s with the smooth aluminium plate. Looking at all the parameter variations, it is noticeable that the phenomena are least noticeable at an oil temperature of 293 K, see Fig. 7 left. The number of droplets decreases significantly and the movement of the droplets is also at a flatter angle to the oil film surface (see Fig. 7). This is due to the higher viscosity of the oil, as the movement of the oil molecules slows down at lower temperatures and the viscosity increases. In addition, a higher temperature leads to a reduction in surface tension as the forces of attraction decrease due to the greater distance between the particles. Consequently, the impulse of the fuel jet and the resulting air flow have a greater influence on the fuel-oil interaction.

To better compare the interactions on different plate surfaces and at different times, the following method is used. Fig. 8 illustrates this procedure using the smooth aluminium plate from measurement series 4.

The first image in Fig. 8 (left) shows the original image. First, the RGB colour channels are extracted for

Tabel 3 Measurement series

	Oil temperature	Oil film thickness	Plate surface
Measurement series 1	293 K	20 µm	smooth aluminium rough aluminium grey cast iron
Measurement series 2		80 µm	
Measurement series 3	363 K	20 µm	
Measurement series 4		80 µm	

Fig. 7 Presentation of the influence of the oil temperature, 293 K (left) and 363 K (right), with an oil film thickness of 80 µm on secondary droplets on a smooth aluminium plate

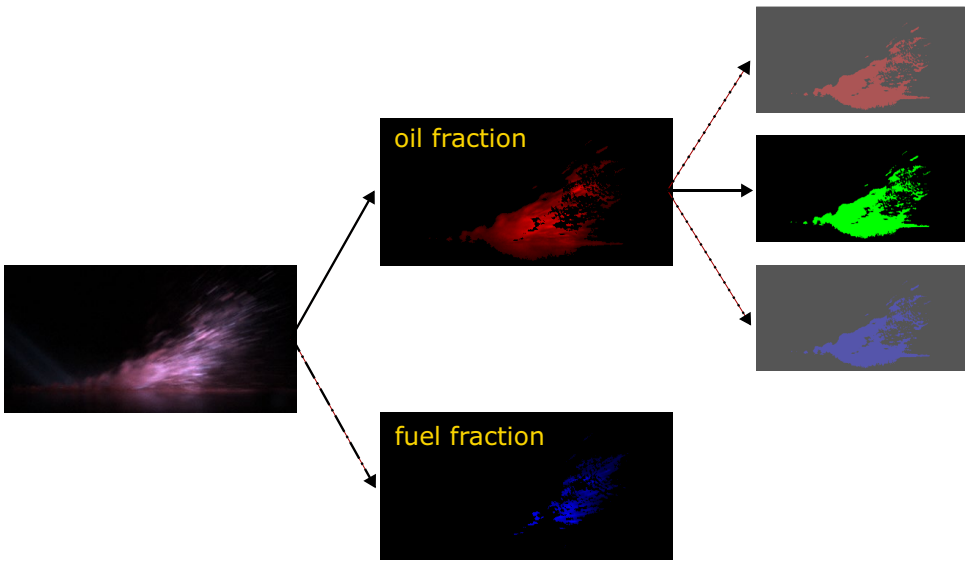

Fig. 8 Schematic workflow for creating the false color representation of the rough aluminum plate (measurement series 4)

all original images of the different measurement series. A threshold of 50 counts is then defined to isolate pixels with an increased red component in the image. A mask is then created that retains only those areas of the image where the red channel exceeds this threshold and dominates over the blue and green channels. The resulting image shows only the isolated red areas, i.e. those that represent a higher proportion of oil. This image is shown along the solid arrow in Fig. 8. Similarly, the blue components of the images are extracted to visualise the fuel distribution during the interaction. This is shown in the lower path in Fig. 8, marked by a dotted line, and leads to the image labelled 'fuel fraction'. The isolated red areas of the original images from the different plate surfaces are then converted into separate colour channels. The first image represents the red channel and corresponds to the images of the smooth aluminium plate. Similarly, the grey cast plate is assigned to the blue channel. As the process is explained in Fig. 8 using the rough aluminium plate as an example, the image representing the smooth aluminium plate and the grey cast iron plate are greyed out. The image for the rough aluminium plate is represented

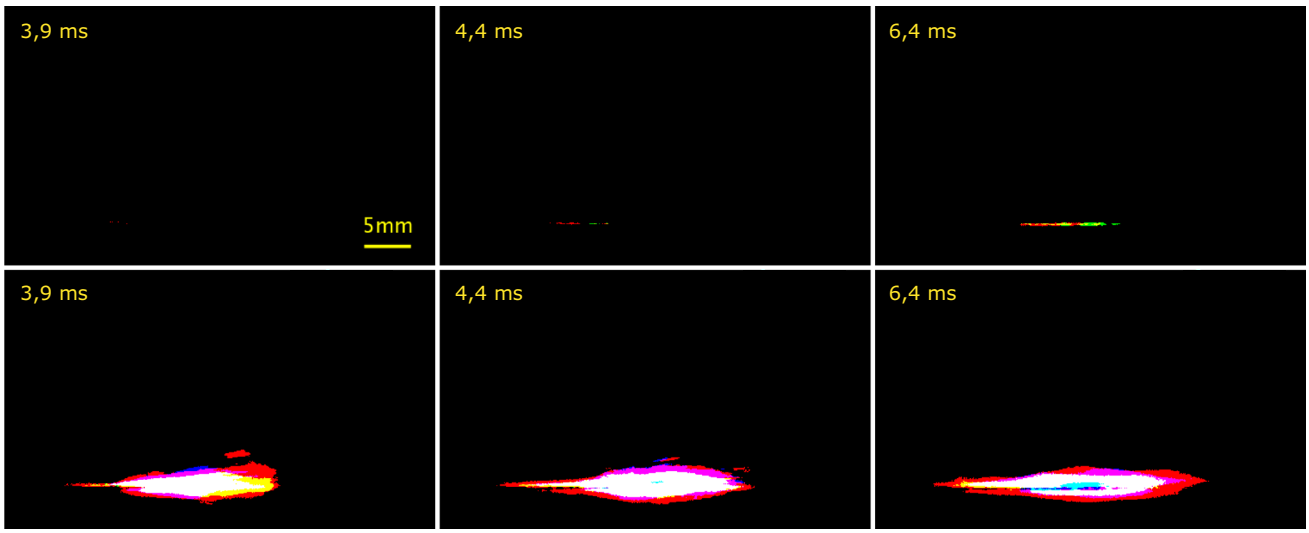

Fig. 9 Influence of the roughness and the plate material on the oil and fuel content at an oil film thickness of 20 µm and an oil temperature of 363 K, red component (top), blue component (bottom)

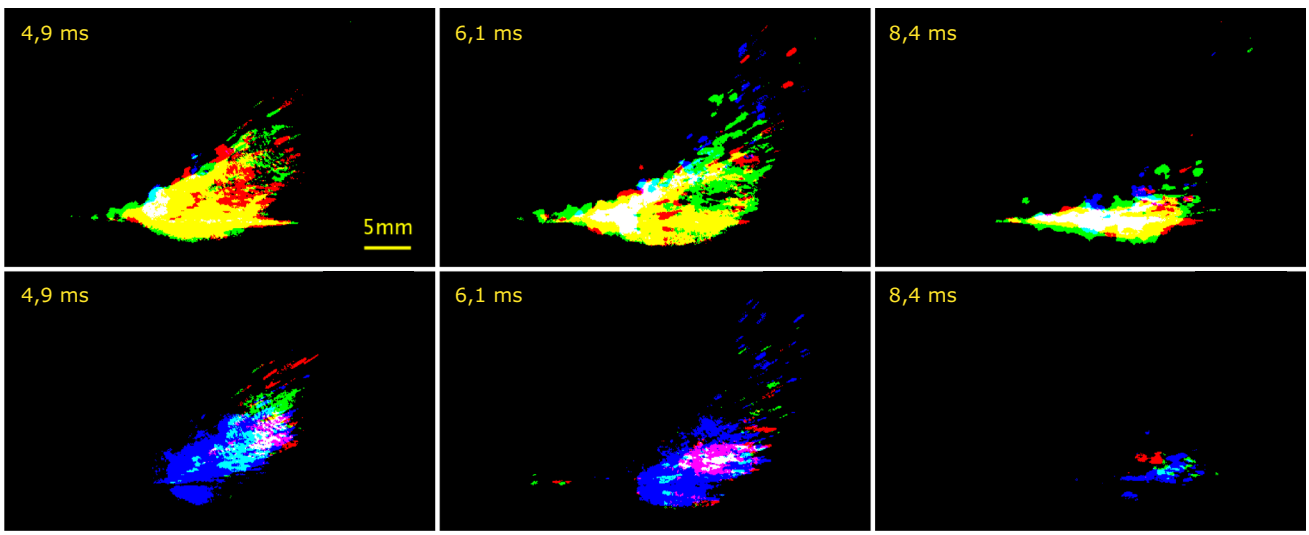

Fig. 10 Influence of the roughness and the plate material on the oil and fuel content at an oil film thickness of 80 µm and an oil temperature of 363 K, red component (top), blue component (bottom)

Tabel 4 Mixed colours created from the red, green and blue components

Mixed color	Red component	Green component	Blue component
White	X	X	X
Violett	X	–	X
Cyan	–	X	X
Yellow	X	X	–
Black	–	–	–

by the green channel. As Fig. 8 illustrates the method for this particular surface, the green image is used along the solid arrow. Combining these colour channels creates a composite image that integrates the isolated red and blue components from the three original images, as shown in Figs. 9 and 10. Superimposing the red, green and/or blue areas in the composite image produces the mixed colours listed in Table 4.

Figures 9 and 10 show the red component of the original polychrome images in the top three images and the blue component in the bottom three images. The images on the left represent the beginning of the interaction, while the images on the right show the time point towards the end of the interaction. The images in the middle show the interaction at an intermediate time. Fig. 9 illustrates the phenomena of measurement series 4, while the phenomena of measurement series 3 can be seen in Fig. 9.

Looking at Fig. 10, it is noticeable that the amount of red on the grey cast iron plate is significantly lower than on the smooth and rough aluminium plate. Correspondingly, less oil detachment occurs on the grey cast iron during the interaction. This is due to the higher adhesive forces of grey cast iron, as explained in 1.2. As a result, the oil film adheres better to the plate surface, resulting in a reduction in oil detachment from the fuel jet. The amount of red on the oil-wetted smooth and rough aluminium surfaces differs little in either amount or shape.

This suggests that roughness has only a marginal effect on the interaction with the same type of material. However, the amount of blue for the grey cast iron plate is significantly higher than for the two aluminium plates, as can be seen from the bottom three images in Fig. 10. The injected fuel accumulates on the surface of the oil film and is then removed by the air flow induced by the fuel jet. Due to the low adhesive forces of aluminium, the injected fuel can interact better with the oil film and the shear force of the air stream is not sufficient to remove the enriched fuel from the surface. The opposite is true for grey cast iron, as the higher adhesive forces make it more difficult for the fuel to accumulate on the oil film. Due to the lower surface tension of the fuel compared to the oil, it can be more easily

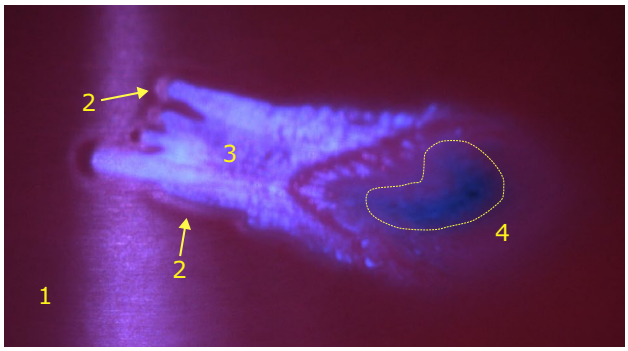

Fig. 11 Macroscopic top view of the interaction area, shortly after injection, 293 K, 80 µm, grey cast iron

detached from the surface by the shear forces of the airflow. The situation is different with a thinner oil film of only 20 µm, as shown in Fig. 9.

As can be seen in the three images above, the red component is very low while the blue component is significantly higher. With a thinner oil film, the polarisation is stronger because the oil molecules are closer to the plate surface. This can also be explained by other adhesion theories, as a thinner oil film allows more direct and effective interactions. This results in a better bond between the oil film and the plate surface, which in turn reduces the amount of oil in the phenomena occurring during the interaction. The smooth aluminium plate has the highest amount of blue, followed by the grey cast iron plate and then the rough aluminium plate. However, this changes at a higher oil temperature of 363 K as the amount of blue for the grey cast iron plate is now significantly higher. This is because temperature has a major effect on the viscosity of the oil film. As the temperature increases, the viscosity of the oil film decreases. At higher temperatures, the shear forces of the airflow are sufficient to dissolve both the fuel enrichments and the oil, so the adhesive forces play a lesser role.

5.2 Investigation of the fuel-oil-interaction after the end of injection

In the following, the interaction on the plate surfaces after the end of injection is analysed using a low-speed camera. Fig. 11 shows an example of the macroscopic top view of the interaction area on the grey cast iron plate in measurement series 2, which is used to describe the phenomena occurring after the end of injection. The structure and composition of the entire interaction area vary depending on the location. Accordingly, there are areas that fluoresce blue, i.e. have a high fuel content, and areas that fluoresce red, with a high oil content, see Fig. 11. It can be concluded that the fuel is deposited on the surface of the oil film and that there is little mixing between the oil and the fuel.

A narrow boundary zone (2) is created between the undisturbed oil film (1) and the interaction zone. This boundary zone, as well as the fuel deposits (3), continue to spread even after the end of injection. This spreading is caused by the kinetic energy of the fuel jet. It can also be seen that the fuel jet causes an almost complete displacement of the oil film at its exit surface, revealing the non-fluorescent plate surface (4). This is the primary area of interaction.

Image subtraction was used to analyse the low-speed images. This allows the difference between several images to be quantified. The first image in a series, the untouched oil film, and the third image, shortly after the end of the injection, were used for this purpose. These images serve as the starting point for the following steps. Each image is converted to greyscale to ensure that the analysis is based on the brightness of the pixels. Next, both images are checked to see if their dimensions match, and if they do not, the second image is adjusted to match the first. This ensures that both images have the same pixel arrangement. The images are now prepared for subtraction and the absolute difference between the grey levels of each pixel between the images can be calculated. The resulting difference image makes it possible to visually identify and interpret the positions and characteristics of the deviations between the two original images. The difference images for different oil film thicknesses and oil temperatures are shown in Figs, 12, 13, 14 and 15. In these figures it can be seen that at a higher oil temperature of 363 K the boundary area becomes larger. The increased area is due to the increased viscosity of the oil film at higher temperatures. It can be seen that although there is a difference in the areas as the temperature increases, there is no discernible difference between the three different plate surfaces. It can be concluded that higher roughness or plate material has no discernible effect on the size of the interaction area. Due to the high impulse of the fuel jet and the low roughness of the plates compared to the oil film, the influence of the different surface topology on the size of the interaction area can be neglected here.

With an oil film thickness of 80 µm and a higher temperature of 393 K, the interface (see Fig. 13) increases significantly compared to a thin oil film thickness of 20 µm at the same temperature (see Fig. 12). With a thicker oil film, there is more oil present, which is more fluid due to the lower viscosity. This allows the oil to spread more easily and farther when it interacts with the injected fuel. A thicker oil film therefore has a much greater effect on the oil/fuel interface at higher temperatures, as there is more oil mass available to expand due to the reduction in viscosity with temperature. At lower temperatures, from 293 K, the interface between oil and injected fuel remains stable due to

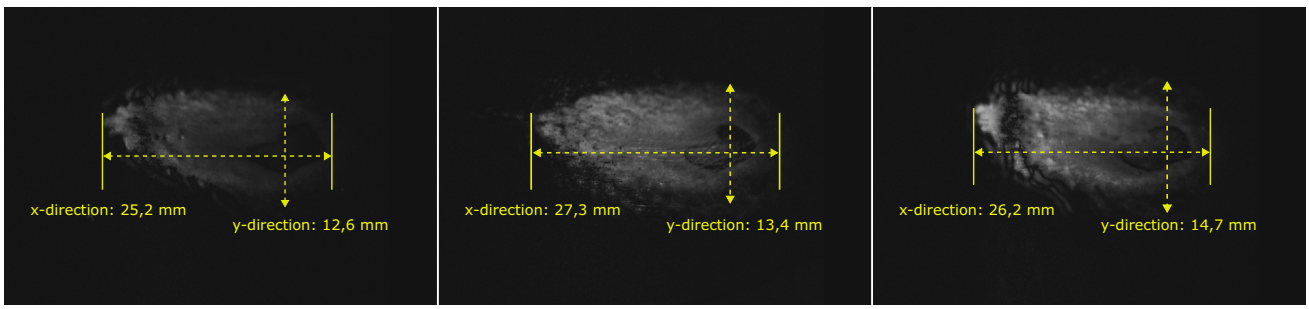

Fig. 12 Influence of roughness and plate material in measurement series 3, smooth aluminium (left), rough aluminium (centre), grey cast iron (right)

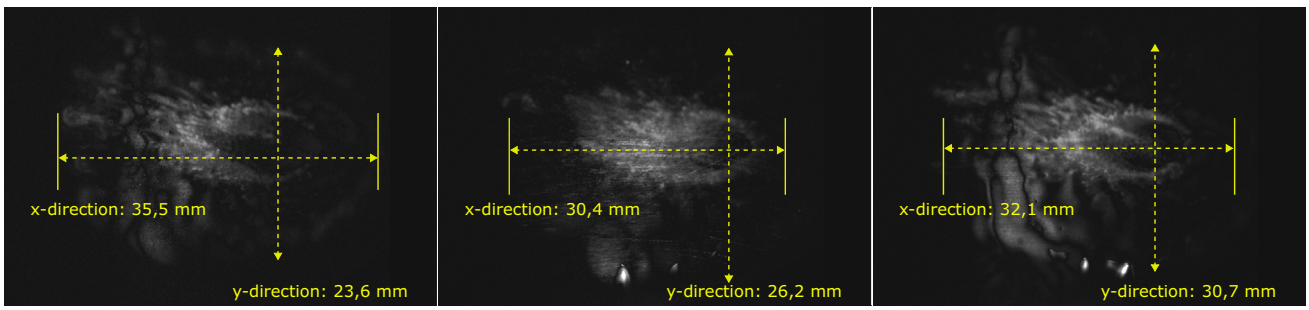

Fig. 13 Influence of roughness and plate material in measurement series 4, smooth aluminium (left), rough aluminium (centre), grey cast iron (right)

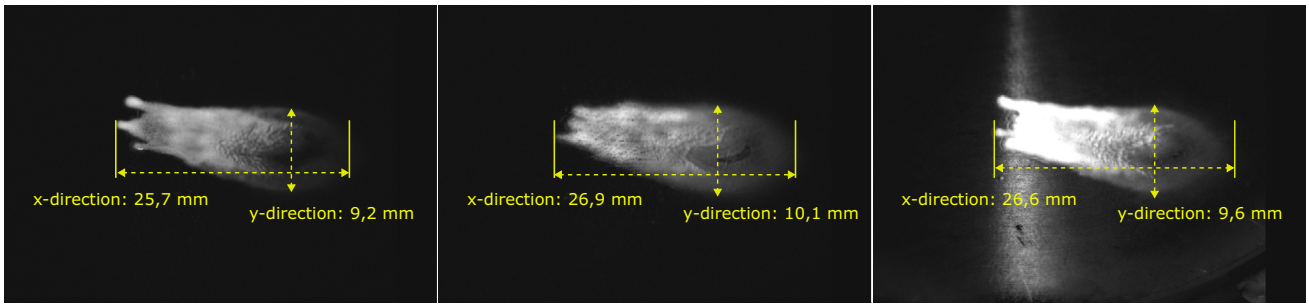

Fig. 14 Influence of roughness and plate material in measurement series 1, smooth aluminium (left), rough aluminium (centre), grey cast iron (right)

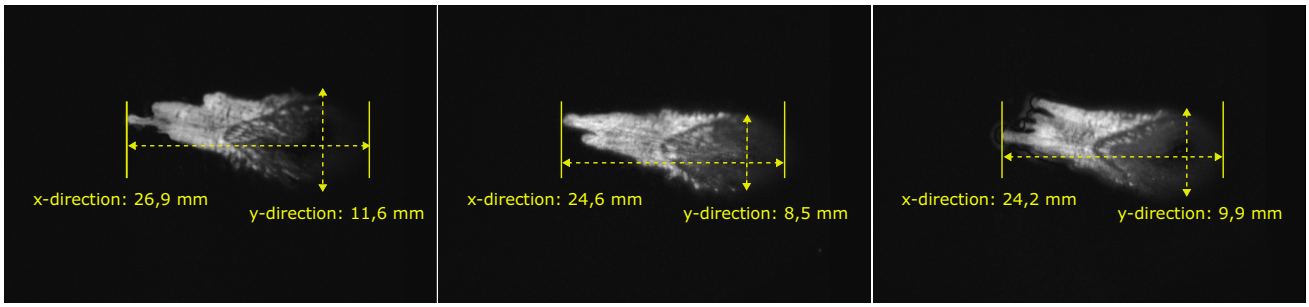

Fig. 15 Influence of roughness and plate material in measurement series 2, smooth aluminium (left), rough aluminium (centre), grey cast iron (right)

the higher viscosity of the oil and shows less expansion, see Figs. 14 and 15. The lower kinetic energy of the molecules leads to stronger intermolecular forces of attraction which restrict the mobility of the oil molecules. This limits the spread of the oil and, therefore, the increase in the oil/fuel interface at low temperatures.

Figures 12, 13, 14 and 15 show that the total interaction range increases from 293 K to 363 K as the oil temperature increases. A direct comparison of Figs. 12 and 14 show that the x-direction range does not increase significantly. In the y-direction there is a noticeable increase from an average of 9.6 mm to 13.5 mm for a 20 µm oil film thickness and from an average of 10 mm to 26.8 mm for an 80 µm film thickness. Due to the lower viscosity of the oil film at higher temperatures, the oil film is more influenced by the impulse of the fuel jet. As the temperature increases, the viscosity of a fluid decreases because the kinetic energy of the molecules increases. This increased kinetic energy reduces the intermolecular forces of attraction by causing the molecules to move faster and further apart. This weakens intermolecular interactions, such as van der Waals forces and hydrogen bonds, as the molecules have greater freedom of movement. As a result, the oil becomes more fluid and can disperse more easily and farther when it interacts with the injected fuel.

6 Summary and conclusions

The presented experiments were performed to investigate the influence of plate surface roughness and chemical composition on the interaction of injected fuel with an oil film. Surface roughness and material properties were systematically varied to analyse their influence on secondary droplet formation, the proportions of oil and fuel during and after the interaction, and the size of the interaction area. Droplet velocity was determined as the central parameter and no significant differences were found between different plate surfaces. The results of the study show that temperature and oil film thickness are critical parameters for the interaction of injected fuel with surfaces. At lower temperatures, the higher viscosity resulted in a lower number of droplets. Higher temperatures reduce the viscosity and surface tension of the oil film, resulting in more intense fuel/oil film interactions and an increased interaction area. Oil film thickness influenced the extension of the interaction area, especially at higher temperatures, as larger amounts of liquid oil interacted more strongly with the fuel. In contrast, the roughness of the same material has only a minor influence. It was found that grey cast iron showed less oil separation than aluminium due to its higher adhesive forces. In the case

of the aluminium plates, the oil separation was comparable regardless of the roughness. This suggests that the material composition and viscosity of the oil film play a much greater role in optimising such processes than the geometric structure of the surface.

Future investigations could look more closely at the influence of different fuel compositions or different oil additives in the oil to gain a deeper understanding of these complex phenomena.

Acknowledgements This work was supported by the Deutsche Forschungsgemeinschaft (DFG – German Research Foundation) Project number 237267381 Collaborative Research Centre/Transregio 150 'Turbulent, chemically reactive, multi-phase flows near walls'. The authors want to thank the DFG for funding this project.

Author contributions C.K., J.R. and M.M. wrote the main manuscript text and all authors reviewed the manuscript.

Funding Open Access funding enabled and organized by Projekt DEAL.

Data availability The datasets generated and analyzed during the current study are available from the corresponding author on reasonable request.

Declarations

Conflict of interest The authors declare no competing interests.

References

1. Willand, J., Daniel, M., Montefrancesco, E., Geringer, B., Hofmann, P., Kieberger, M.: Grenzen des Downsizing bei Ottomotoren durch Vorentflammungen. MTZ Motortech Z **70**(5), 422–428 (2009). https://doi.org/10.1007/BF03225495
2. Schweizer, T., Zöbinger, N., Kubach, H., Lauer, T., Koch, T.: Experimental and numerical low-speed pre-ignition analysis and mechanism synthesis on a turbocharged gasoline engine with direct injection, *SAE Int*. J. Engines (2023). https://doi.org/10.4271/03-16-03-0018
3. Singh, E., Ali, MJ., Ichim, A., Morganti, K., Dibble, .: Effect of Mixture Formation and Injection Strategies on Stochastic Pre-Ignition. *SAE Technical Paper Series*, 2018-01-1678, (2018). https://doi.org/10.4271/2018-01-1678
4. Maliha, M., Stumpf, B., Beyer, F., Kühnert, M., Kubach , H., Roisman, I., Hussong, J., Koch, T.: Optical investigation on the interaction between a fuel-spray and an oil wetted wall with the focus on secondary droplets. Int. J. Engine Res. **24**(4), 1578–1588 (2023). https://doi.org/10.1177/14680874221095235
5. Risse, A.: *Fertigungsverfahren der Mechatronik, Feinwerk- und Präzisionsgerätetechnik*. Vieweg+Teubner Verlag, Wiesbaden (2012)
6. Kubišová, M., Knedlová, J., Vrbová, H., Pata, V., Bočáková, B.: Statistical evaluation of hard-to-measure surfaces. J. Phys. Conf. Ser. **2712**(1), 12020 (2024). https://doi.org/10.1088/1742-6596/2712/1/012020
7. Flock, D.: Wärmeleitungsfügen hybrider Kunststoff-Metall-Verbindungen. Aachen, Techn. Hochsch., Diss., 2011. Aachen: Publikationsserver der RWTH Aachen University (2012)
8. Schlitt, C.: Thermoplasten und Flüssigsilikonen mit unterschiedlichen Mechanismen zur Initiierung der Vernetzung hergestellt im Mehrkomponenten-Spritzgießverfahren. Kassel, Universität Kassel, Diss., 2018. Kassel: Kassel University Press GmbH (2018)
9. Brockmann, W., Geiß, P.L., Klingen, J., Schröder, B.: Klebtechnik: Klebstoffe Anwendungen und Verfahren Klebtechnik. Wiley, Hoboken (2005)
10. Deters, L.: Reibung Verschleiß und Schmierung. In: Sauer, B. (ed.) Springer-Lehrbuch. *Grundlagen von Maschinenelementen für Antriebsaufgaben,* 8th edn, pp. 1–68. Springer Vieweg, Berlin (2018)
11. Chu, N.R., Jackson, R.L., Ghaednia, H., Gangopadhyay, A.: A mixed lubrication model of piston rings on cylinder liner contacts considering temperature-dependent shear thinning and elastic-plastic contact. Lubricants **11**(5), 208 (2023). https://doi.org/10.3390/lubricants11050208
12. Habenicht, G.: Bindungskräfte in Klebungen. In: Habenicht, G. (ed.) Lehrbuch, *Kleben - erfolgreich und fehlerfrei: Handwerk, Praktiker, Ausbildung, Industrie,* 7th edn., pp. 69–76. Springer Vieweg, Wiesbaden Heidelberg (2016)
13. Häntsche, J.P.: Entwicklung und experimentelle Untersuchung einer Hochdruckpumpe für Ottokraftstoff basierend auf ingenieurkeramischen Gleitsystemen. Zugl: Karlsruhe Univ. (TH), Diss., 2009. Berlin: Logos-Verl (2010)